Construction of Patient Specific Virtual Models of Medical Phenomena

Božidar Potočnik, Dušan Heric, Damjan Zazula, Boris Cigale and Daniel Bernad
University of Maribor, Faculty of Electrical Engineering and Computer Science
Smetanova 17, 2000 Maribor, Slovenia
E-mail: bozo.potocnik@uni-mb.si

Tomaž Tomažič
Teaching Hospital of Maribor
Ljubljanska 5, 2000 Maribor, Slovenia

Keywords: virtual medical model, image processing, modelling, simulation

Received: February 10, 2004

A framework for construction of virtual models of the medical phenomena is proposed. Major construction steps are discussed in detail. The construction of virtual medical model is guided from acquisition of patient imaging material, to 3D reconstruction based on the image processing, to the basic modelling and simulation approaches. This framework is demonstrated on human knee joint virtual model construction. Statistical assessment of the built knee joint model points out sufficient quality and accuracy. Model assessment from clinical point of view confirmed this evaluation, and, simultaneously, verified the proposed construction chain as very prospective.

Povzetek: Razvita je metoda za prikazovanje medicinskih pojavov na pacientovem kolenu.

1 Introduction

Atlases and 3D human organ models for "typical" patient do not suffice in a modern medical practice anymore. Successful diagnosing and decision-making in medicine today is unavoidably dependent on relevant patient specific information. Such information is mainly extracted by using non-invasive methods like medical imaging techniques, e.g. ultrasonography and magnetic resonance (MR) imaging. Furthermore, a need to adapt atlases and organ models for specific patient anatomy emerged. This need is intensified when planning surgeries. Surgeons namely face a problem when imagining a detailed surgery in advance, although having MRI recordings at their disposal, for example. They lack a model that would offer a virtual walk through the tissues and organs, and maybe an option of virtual testing of some specific surgery detail. A desired solution, of course, must incorporate a thorough and reliable computer support, which is not available in today's medical devices and computer software.

The models of organs, appropriate for surgical planning, should be available in their close-to-natural constellation either for individual usage, i.e. each organ separated from the others, or for grouping them together in arbitrary combinations. The obtained computer models should be aimed at any virtual (spatial) inspection and scanning along arbitrary cross-sections in all directions. The most desired option is a kind of virtual travel through models, possibly equipped with a collision detection module. The most challenging feature of such models is, however, virtual surgery.

A generic procedure for constructing virtual medical models is presented in this paper. After a survey of related work in Section 2, major construction steps are outlined on an example of human knee joint in Section 3. Section 4 presents simulation results and quantitative assessment of quality for constructed models, followed by a discussion section which emphasises current modelling approaches and potential difficulties with the process of construction. Our conclusions also stress the applicative value of such models in the clinical practice. The present work summarizes a part of the SimBio project results [15].

2 Related work

Current state of the art in the computer science and medical devices already enable individualisation of patient data processing. Various approaches to biomedical image processing, object recognition, and reconstruction have been developed [2, 5, 6, 12]. None of those methods cited is, however, general and equally applicable in different situations. On the other hand, medical imaging devices are daily used for patient diagnosis. Such examinations are relatively low-cost. The technology thus assures all possibilities for construction of virtual medical models.

There already exist few solutions for the medical field, where majority deal with an organ reconstruction/visualisation and virtual inspection. Reference [17] brings comprehensive review on this topic, while [7] describes virtual endoscopy as an example of virtual organ inspection. Some models tackled a virtual surgery, especially a surgical planning [9, 20]. There exists also other appli-

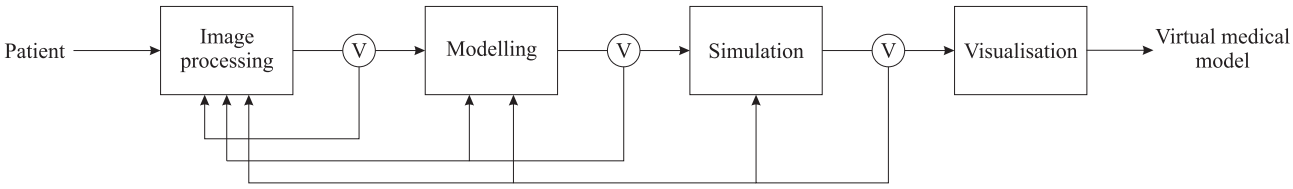

Figure 1: Major steps for construction of virtual medical model. Verification procedure (encircled V) refines particular construction steps.

cations of these models. For example, in [3, 8] models are used as virtual training systems in the medicine, while in [11] they are used for a construction of organ atlases. Although, above mentioned solutions are effective on fields for which they were developed, it can not be affirmed that they are general or generic. Also the construction procedure it is not generic. These models are not complete as well, because they cover just some viewpoints (e.g. just surgical planning and not actual virtual surgery).

3 Method: measurement, modelling, and simulation

In the sequel, we propose a procedure for construction of virtual models of the medical phenomena. Figure 1 depicts a construction procedure with all major building blocks. The construction of virtual medical model is guided from the initial step, i.e. acquisition of patient imaging material (Subsection 3.1), followed by the description of 3D reconstruction based on the image processing (Subsection 3.2), to the basic modelling-simulation approaches and directives (Subsection 3.3). It can be seen from Figure 1 that the results of verification/validation (denoted by the encircled letter V) influence the previous steps. They actually help to refine object detection, modelling, and simulation, and, consequently, constructed virtual medical model. This description is substantiated by example of the human knee joint virtual model construction. Results are taken from the SimBio project [15]. The SimBio project is an example of the proposed construction procedure defined in Figure 1.

3.1 Acquisition of imaging material

The first step in construction of virtual models is to acquire patient specific anatomy. This is usually achieved by non-invasive imaging methods. It is essential to acquire high-quality imaging material, because all other construction steps depend upon it (see Figure 1).

We deal with a human knee joint anatomy in our example. Figure 2 depicts the knee joint with three main bones– bone femur, bone tibia, and bone patella. Our intention is to observe these bones with their belonging cartilages and menisci (both lateral and medial), while all other structures in the knee joint are insignificant.

Important parts of patient anatomy indirectly narrow a set of potential medical imaging devices. The MR imaging technique was chosen to achieve our aim. We have access to the Toshiba Visart 1.5T MR scanner. Knee joint was imaged with different settings of the MR scanner parameters, such as image technique, flip angle, field of view (FOV), slice thickness, imaging timing parameters (TR and TE), number of acquisitions (NAQ), size of output matrix, etc. MR scanner parameters were selected in order to emphasise boundaries between bones, cartilages, and menisci, and, at the same time, retain adequate resolution for subsequent 3D reconstruction. It should be noted that altering scanner parameters always alters image quality, which is in proportion to the acquisition time. The selected MR scanner parameters were: FE3D image technique with QD knee coil, TR was 41 ms, TE was 9.0 ms, flip angle was fixed at 18/73, NAQ was 1, effective pixel size was 0.4 mm, FOV was 22 x 22 cm, and the output image matrix was 512x512 pixels. The number of images (slices or cross-sections) in the sequence was 60 with 2 mm slice thickness. Acquisition time was around 22 minutes.

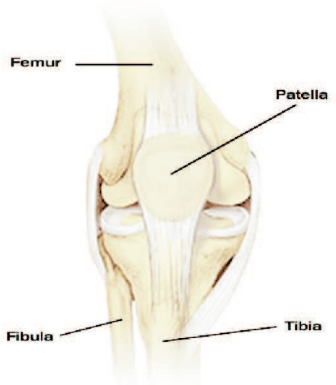

Figure 2: Human knee joint with ma3n bones.

3.1.1 Additional patient-specific information acquisition

If realistic object reconstruction is sought, then it is mandatory to keep sufficient spatial and lateral resolution of patient imaging material. Sometimes also other patient information is necessary. The reason can be twofold, namely, additional information can be mandatory for modelling procedure, or can be used for the verification/validation of

behaviour of constructed virtual models.

Our sample virtual medical model should imitate kinematics in the human knee joint. Additional information, as for instance the force in the knee, and examples of real knee kinematics are thus required. The patient should be examined when performing a gait cycle to acquire the most representative values. This can be achieved in an expensive open MRI scanner. Therefore, we seek an alternative solution. We designed a special MR compliant exercise rig to record the gait cycle and forces. The MR rig allows a volunteer or patient to undertake a controlled exercise protocol while exerting known light forces. This rig is fully MR compliant–it does not utilise any metal or ferromagnetic materials in its construction. Wooden part of this rig–i.e. pedal–was basically constructed according to [10] and, afterwards, modified to enable setting of 6 different knee flexion angle positions. Angles vary with respect to the patient's leg length, but generally are in the range from 0 to 40 degrees flexion with 8 to 10 degrees increments. Figure 3 (a) depicts this pedal. Particular knee angle position can be selected manually during MR imaging by adjusting a wooden coil. The pedal expanse is limited by the MR scanner bore dimensions. Maximal knee flexion angle supported is thus around 60 degrees.

Patient with flexed knee pushes against the wooden pedal during MR imaging. This force is measured with a special optical force measuring system which was also developed. A core of this system is a force sensor, which utilizes a simple principle of measuring the optical power losses in optical fibre caused by bending the fibre. The fibre multi-loop coil is positioned between two walls of the force sensor case (see Figure 3 (b)), separated by elastic spacers (rubber). The applied force causes displacement of the movable sensor case wall that bends the optical fibre coil and induces decreasing of the passed optical power. Alteration in optical power is afterwards transformed into a force value, which is displayed and stored by PC-based monitoring system. Figure 3 (c) depicts a volunteer during the acquisition of specific parameters by using the described MR-compliant exercise rig.

If additional patient-specific information except imaging material is required, then it is reasonable to simultaneously record all patient data and images. Possible errors in subsequent modelling are minimised in this way.

3.2 Image processing and 3D reconstruction

The next step after acquiring patient imaging material is to build 3D models of the observed organs or tissues (see Figure 1). This anatomy is usually obtained by applying 3D reconstruction on image segmentation results. The object recognition encompasses in general three major steps: preprocessing, segmentation, and object classification. Preprocessing either removes artefacts from images and/or enhances particular object features. The aim of image segmentation is to group pixels (voxels) with similar features into potential objects (bodies). Finally, an object classification discriminates between actual objects, background, and noise by using some criteria function.

There is variety of segmentation methods applicable for medical image sequences [14], either designed for 2D object detection in particular image (cross-section) from the sequence or 3D detection where image sequence is treated as a whole. Despite heterogeneity of methods, there are some directives applicable for method selection. First, a decision between automated or semi-automated segmentation should be taken. Although automated object recognition is preferred, it should be used with caution; namely, the obtained results must always be thoroughly verified. On the other hand, the semi-automated segmentation requires a clinician interaction during the processing, and verification is normally not necessary.

Segmentation methods are classified into three major groups [16]: a) pixel based or thresholding, b) contour or edge based, and c) region based methods. Selection of segmentation method depends primarily upon image modality (e.g. ultrasound, MR, positron emission tomography–PET) and the type of searched objects. If boundaries between objects and background are distinctive and well-defined, then methods from all three groups are potential candidates. If boundaries or edges are, however, weak, then thresholding and edge-based methods will not perform well. In real applications, the segmentation is a combination of all three major groups. On the other hand, the image modality defines the quality of boundary and potential artefacts (noise) in images. In ultrasound images, for instance, it is known that edges are not expressed and that speckle noise is present [13].

Object recognition procedures are designed to detect objects with special features. It is therefore common to include a prior-knowledge about objects and image modality in this recognition process. There are two possibilities for considering the prior-knowledge: a) segmentation method is context-based, b) classification is context-based. The first option means that segmentation method favours regions with pre-described shape and features (e.g. expected size, mean grey-level, compactness, and texture). On the other hand, the context-based classification extracts objects out of all regions obtained by segmentation according to some defined criteria. Criteria encompass prior-knowledge, while the segmentation method treats all regions equally in this process.

A big problem of object detection procedures is that they are not portable between medical imaging devices of same type but from different vendors (e.g. Philips MR scanner and Toshiba Visart MR scanner). Recognition process is usually developed by analysing the imaging material from a single device. The variability inherent when using different imaging devices is therefore not taken into account. Parameters of medical imaging device (see Subsection 3.1.1) are limited and, thus, theoretically could not be uniformed for all devices. Quality recognition process should therefore not be founded on grey-level features, but potentially on the contrast invariant features.

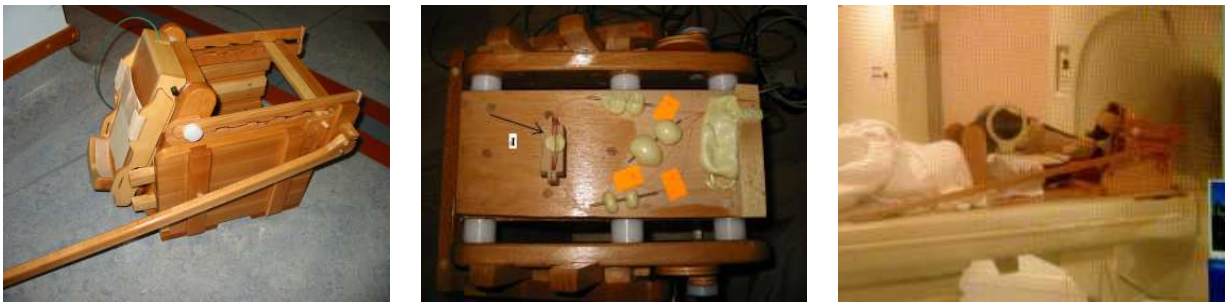

(a) (b) (c)

Figure 3: MR compliant exercise rig: a) wooden pedal, b) optical force sensor integrated on pedal, c) volunteer during additional parameter acquisition in the MR scanner.

The next step after segmentation is 3D object reconstruction. The reconstruction builds a 3D object model from partial segmentation results obtained on slices (cross-sections). Competent reconstruction supposes accurate segmentation and exact position of each slice in the 3D world or sufficient knowledge about image forming. Parallelism of subsequent cross-sections in the sequence greatly simplifies 3D reconstruction. In this case, it is mandatory to know exact inter-slice distance. If all conditions at image acquisition are not known or if even medical imaging device is not capable to return all these parameters, then the object reconstruction can only be informative. Figure 4 depicts a poor 3D reconstruction of two follicles from ultrasound ovarian image sequence obtained by intra-vaginal probe. This reconstruction mis-assumed that cross-sections are parallel; in fact, all cross-sections have common origin (i.e. probe) and an angular displacement between two subsequent cross-sections is constant. This displacement is, however, not possible to obtain from 2D ultrasound scanner used in this example. This indicates that not all medical problems could be accurately reconstructed.

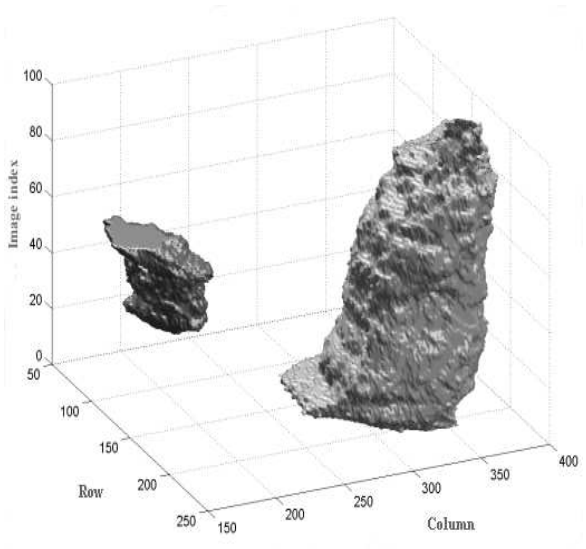

Figure 4: Poor 3D follicle reconstruction from 2D ultrasound ovarian image sequence.

3.2.1 Registration of MR knee images and 3D reconstruction

Image sequences from our human knee joint example are segmented by using a non-linear registration or mapping, respectively. Registration method was applied for two reasons: a) weak edges of knee structures, and b) simple and efficient integration of prior-knowledge (e.g. definition of relations between bones and cartilages, narrowing searching region). A patient knee image sequence is actually registered to a template knee image (sequence). Template knee image is constructed only once and is immutable in the registration process. It was constructed from knee image sequence of a typical patient. Each knee structure was accurately annotated on every MR slice. These readings actually define relations and approximate positions of bones, cartilages, and menisci in the human knee. The registration algorithm applied is based on the following registration equation [19]:

$$f - m = \frac{1}{2}[\triangle u(r)\frac{\partial f}{\partial u(r)} - \triangle u(r)^{-1}\frac{\partial m}{\partial u(r)}], \quad (1)$$

where f is the fixed or template image, m is the moved or patient image, $\triangle u(r)$ is the mapping function which maps m to f, and $\triangle u(r)^{-1}$ is the inverse function which maps f to m. Making the assumption that $\triangle u(r) \approx -\triangle u(r)^{-1}$ and gradient of $f \approx$ gradient of m, it is possible to reduce this equation to either of the following:

$$f - m = \triangle u(r)\frac{\partial f}{\partial u(r)} \quad \text{or} \quad f - m = -\triangle u(r)\frac{\partial m}{\partial u(r)}.$$

A quality measure for goodness-of-fit between both images is based on sum-of-squares of differences of voxel grey-level intensities. Full details of this registration routine will be published elsewhere.

This registration routine results in a mapping function (see Eq. (1)). Mapping function can be used to map readings (e.g. bone femur) from the template image sequence

to the patient image sequence. These partial results can be afterwards used for 3D reconstruction. Performing reconstruction this way is possible and valid, however, it introduce some artefacts. Disturbing staircase pattern (i.e. terracing problem) is frequently noticed in transitions from slice to slice. Another reconstruction approach was therefore followed. First, the 3D template knee model was developed from template image by using manual annotations. This template model was afterwards mapped by the calculated mapping function and, thus, the patient 3D knee model with sufficient quality is obtained.

Template knee model was constructed by using a combination of tools [15]. This knee model is actually finite element (FE) 3D mesh. First, the SURFdriver 3.5 software [18] was used to hand segment three bones, the belonging articular cartilage surfaces, and both menisci. The 3D surface points for each of these structures were then imported into Ansys meshing software [1], where meshes were manually refined. From a FE point of view the bones themselves are considered as rigid body structures. Bones were then passed from Ansys into Matlab environment, where the articular cartilage was generated using the registration algorithm described above. The outer surface of the bone structure was morphed onto the outer surface of the cartilage, and a set of 3D 8-node elements were created using this mapping. The smoothness constraints in the registration algorithm ensure that these elements have an acceptable geometry for analysis and simulation.

Described registration and mapping of template knee model produce high-quality patient-specific FE 3D knee meshes as shown in Figure 5.

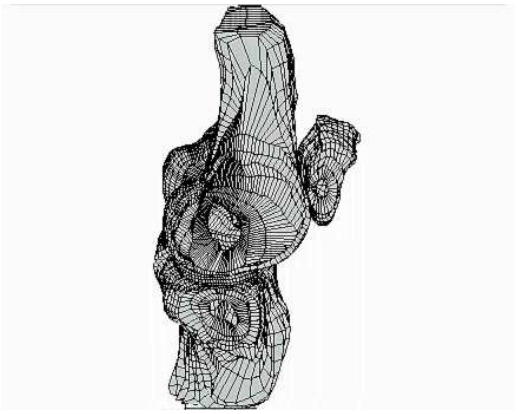

Figure 5: Patient-specific FE 3D knee mesh.

3.3 Modelling and simulation

Reconstructed human organs and tissues are usually presented in a form of surface meshes. Surface is formed from 3, 4 or 6 connected vertices, which consequently defines triangular, tetrahedral or hexahedral mesh. The aim of modelling phase (see Figure 1) is, however, to imitate the functionality of organs. An appropriate virtual model needs thus to be set. Many real-world properties must be linked to surface meshes of reconstructed objects. The information about the object's material properties (e.g. stiffness, friction) is mandatory. To imitate kinematics it is necessarily to prescribe the trajectory of movement for all objects and their interdependence. For complete virtual model it is also required to define scenarios of model behaviour in different situations.

Many general purpose modelling and simulation tools are available on the market to simplify this development (e.g. MSC.Software Suite, PAM Suite, ABAQUS). Besides, it is possible also to develop own modelling-simulation tools specially adjusted for specific problems–for instance a virtual delivery room simulator in [8]. Commercial tools are usually well tested and documented, with good technical support, and extensive consumer list. However, their drawbacks are usually limited options of a tool and, of course, high price. On the other hand, special designed software can support all options required, but on an expense of lengthy development and poorer validation/verification.

Virtual model of human knee joint was built by a commercial modelling/simulation software PAM Suite [4]. PAM Suite is actually a bundle of three products: a modelling tool Generis, a finite element problem solver or simulator Safe, and a visualisation tool View. The kinematics of reconstructed patient knee joint–represented in a form of FE surface meshes–was thus modelled by the PAM Generis. Four major sub-problems were addressed in the modelling phase: a) assigning appropriate material properties to each knee structure, b) design of accurate MR exercise rig model (foot-pedal), c) applying correct force on foot-pedal, and d) definition of the knee structure interdependence.

Several material properties like density, shear, yield stress, bulk modulus, Poisson's ratio, linear elastic stiffness, and coefficient of static friction are assigned to each knee structure. The parametric values were carefully selected [15]. It is known that some material properties are changed by temperature alteration and by patient aging. Nevertheless, we simplified our model and assigned the same property values to all patients.

A MR compliant exercise rig (see Subsection 3.1.1) was used during a patient imaging material acquisition. Its purpose was to mimic and partially record the conditions during a gait cycle (i.e. acquisition of forces and angles between the major knee bones). The simplified rig model as shown in Figure 6 (b) was added to human knee joint model. The foot-pedal is modelled by 3 and foot beams by 7 bars. A bar is a special element defined by two nodes and some material properties. All movements around these two nodes are possible. However, only forces in the direction of the bar can be applied.

Three main knee bones and fibula are defined as rigid bodies to avoid deformations. Their shape is completely described by the reconstructed FE surface mesh. Ligaments and muscles are manually added to the knee model.

They are used to define interdependence of bones and, consequently, enable the knee kinematics (i.e. knee extension/flexion). They are modelled as bars (see Figure 6 (a)). Quadriceps muscles and tendons (label 1) are modelled by 3 bars, while hamstring (label 2) is modelled by 2 bars, where one bar is connected to the fibula and the other on the tibia. Patellar ligament (label 3) consists of 5 bars linking the patella with the tibia. Lateral and medial collateral ligaments (label 4) are modelled by 4 bars on each side of the knee. They are main links between the femur and tibia (or fibula). Bars are also used to fasten menisci to the tibia. Without these bars, the meniscus remains in its initial positions during the simulation. Anterior and posterior cruciate ligaments are also modelled by bars. They ensure the knee stability.

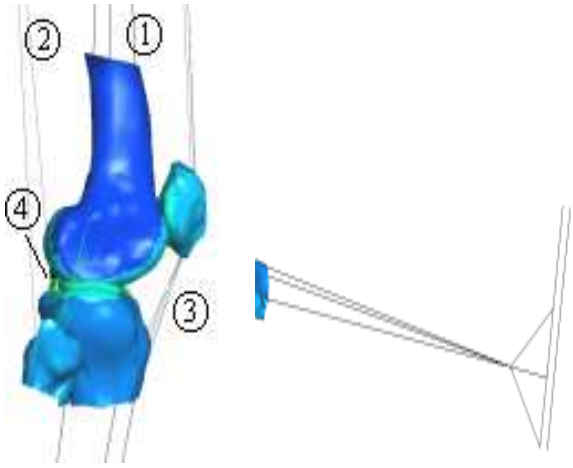

(a) (b)

Figure 6: Finite element models: a) knee model, b) MR exercise rig model

The whole leg must be modelled to simulate a patient pushing against the foot-pedal of the rig. Missing parts of the bone femur and tibia are modelled by 3 bars each. These bars join in a common node, which enables rotation of both bones in every direction. MR exercise rig model (see Figure 6 (b)) is connected to the node, where bars representing the tibia meet. The footplate points are restricted to translate exactly as the foot is. To simulate the knee flexion during a gait cycle, it is necessary to apply a correct force on the foot-pedal. This force is concentrated in a point of the foot-pedal; its value was, however, obtained during the patient MRI examination.

The modelling phase is followed by the simulation (see Figure 1). The obtained patient-specific knee model is afterwards simulated by using the PAM Safe tool. No manual interaction is required during the simulation. PAM Safe offers a very useful option to track the position of elements (e.g. node) or observe forces during the simulation. The simulation results in the simulated knee flexion ranging from fully extended knee to the knee flexed around 90 degrees. Results can be visualised by the PAM View tool.

4 Results

Efficiency of the built knee joint model will be presented in this section. This model actually simulates knee kinematics during a gait cycle under different scenarios. It is possible, for instance, to remove anterior crucial ligaments or simulate broken meniscus by the modelling tool PAM Generis and, consequently, observe knee kinematics of the altered knee anatomy. Results are visualised by the PAM View tool. It is possible just to observe knee kinematics in a form of animation movie with graphical manipulation option (e.g. rotation of the field of view, removing some uninteresting structures), or observe the results on a detailed level of nodes and forces. Figure 7 depicts the simulation results for the human knee joint model from its initial, extended, position to the final position of fully flexed knee.

There are 3 validation/verification milestones foreseen in the process of virtual model construction as seen from Figure 1. However, it is impossible to verify solely the modelling phase of our sample construction process. Verification is thus performed on 2 spots only–after image processing and simulation phase. Results after image processing (and reconstruction) phase are usually 3D surface meshes for particular structure. Figure 5 depicts surface meshes for reconstructed MR knee joint (see Subsection 3.2.1). These intermediate results must be compared to the correct real-world circumstances in order to assess the accuracy of reconstructed surface meshes and, indirectly, also the quality of segmentation-reconstruction process. The most competent verification relies on construction of virtual model for a phantom (e.g. phantom of the human knee joint). In the verification phase, the obtained model and also all intermediate results (e.g. surface meshes) are compared to the phantom. Usually, there are no phantoms available or they are very expensive. The most widespread verification technique is thus to compare the reconstructed surface meshes with the data provided by several experts. Experts usually manually annotate all important structures through entire image sequence. Afterwards, the so called "mean expert" annotations are calculated, thus minimizing inter-observer variability. These annotations are then used to build the experts' surface meshes, which are compared with the reconstructed surface meshes.

We performed twofold verification: a) 3D verification, where the reconstructed meshes are statistically compared to experts' (orthopeadic surgeons) meshes, and b) 2D verification, where the reconstructed meshes are first cut through and, the obtained contours are, afterwards, compared to experts' manual readings for a particular slice. The Haussdorf distance (HD), the mean absolute distance (MAD), and the spherical distance (SD) as a generalization of MAD distance for the 3D space, are measured between the experts' and segmentation-reconstruction results. Table 1 depicts the average distances calculated for surface meshes of 6 patients. Three major bones and their corresponding cartilages are verified. A bigger distance indicates a bigger error of the registration-reconstruction pro-

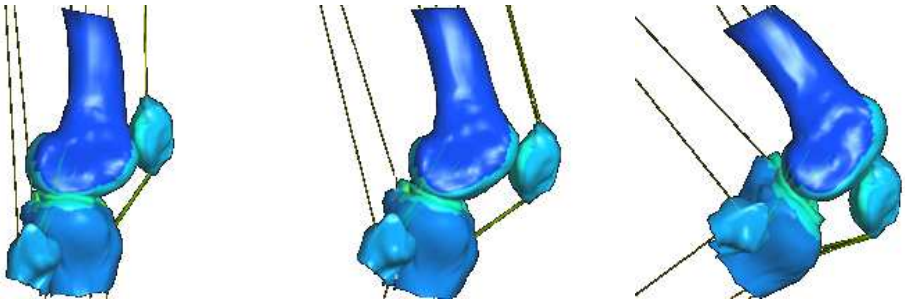

(a) (b) (c)

Figure 7: Simulated knee kinematics: a) initial knee position (simulation cycle 0), b) knee flexed around 45 degrees (cycle 150), c) fully flexed knee (cycle 300).

cess. The HD distance measures the biggest distance between two corresponding points from two curves, while the MAD distance returns an average distance between two curves. The HD distance is thus always bigger than MAD distance. The obtained results point out sufficient quality for subsequent construction phases. Also the visual inspection of these intermediate results performed by orthopeadic surgeons confirmed a good accuracy through entire image sequence (if the contours are observed). The biggest error is noticed on both extreme sides of a particular knee structure, where this structure begins to emerge or sink. These regions are very unexpressed and, therefore, present a huge problem for registration routine.

	MAD (mm)	HD (mm)	SD (mm)
BF	1.51	7.98	4.81
BT	1.48	7.34	3.66
BP	1.42	6.03	2.42
CF	1.32	9.41	7.62
CT	0.92	4.92	2.13
CP	1.22	6.07	2.65

Table 1: Statistical assessment of registration-reconstruction process for three bones (BF–femur, BT–tibia, and BP–patella) and their corresponding cartilages.

Calculated knee surface FE meshes are afterwards used in the modelling and simulation procedure as described in Subsection 3.3. Visual inspection of the final virtual human knee joint model performed by clinicians was focused on the relations and deformations of articulating bodies during the knee flexion. In general, the articular proportions in the simulated knee joint are very clear. No obvious and non-physiological structure deformations, with exception of slight patella gliding disturbances, are noticed.

As a quantitative verification measure of the model quality, three Euler rotation angles for bone tibia with respect to bone femur are observed–i.e. rotation around X axis (varus/valgus), around Y axis (internal/external rotation), and around Z axis (flexion/extension). It is known that during a gait cycle both major knee bones experience some translation and rotation with respect to their initial position. The measured rotations in the X, Y, Z directions of the tibia relative to the femur derived from the MR images are thus compared to the modelled rotations. Measured angle values are calculated from low-resolution MR knee images acquired by using MR exercise rig (see Subsection 3.1.1). Patient was additionally imaged in 6 flexion positions of knee. Image sequence acquired at a particular knee flexion angle was, afterwards, registered to bone femur and bone tibia surface meshes (volumes). This registration results in affine matrix which can be decomposed into required Euler rotation angles. Three Euler rotation angles can also be calculated from the simulation results. Twenty nodes from each major bone are traced during the simulation. For the i-th cycle, the following 4x20 matrix is defined:

$$\mathbf{X_i} = \begin{bmatrix} x_{i,1} & x_{i,2} & & x_{i,20} \\ y_{i,1} & y_{i,2} & & y_{i,20} \\ z_{i,1} & z_{i,2} & \cdots & z_{i,20} \\ 1 & 1 & & 1 \end{bmatrix},$$

where triplet $(x_{i,j}, y_{i,j}, z_{i,j})$ present coordinates for the j-th node in the i-th cycle. Usually, there was 300 simulation cycles. Then, the following predetermined linear equation system must be solved:

$$\mathbf{X_i} = \mathbf{A}_i \mathbf{X}_0,$$

where $\mathbf{X_0}$ denotes a matrix with the initial bone position (at cycle 0), $\mathbf{X_i}$ denotes a matrix with the bone position at cycle i, and $\mathbf{A_i}$ denotes the affine matrix in cycle i. After calculating affine matrices for all cycles for both bones, a new affine matrix of tibial flexion position with respect to femur is calculated in each cycle as follows:

$$\mathbf{J_i} = \mathbf{T_i^{-1}} \mathbf{F_i},$$

where $\mathbf{T_i}$ and $\mathbf{F_i}$ denote affine matrices in the i-th cycle for bone tibia and femur, respectively. This affine matrix takes the form of:

$$\begin{bmatrix} & [\mathbf{R}] & & [\mathbf{L}] \\ 0 & 0 & 0 & 1 \end{bmatrix}.$$

The Euler angles for each simulation have been calculated from the 3x3 rotation matrix, $\mathbf{R}$, and the translation vector, $\mathbf{L}$.

A comparison between the measured and Euler rotation angles obtained from the simulation pointed out a small difference in X and Y direction at fixed Z angle. This difference varied up to 10 degrees [15]. These results confirmed the virtual human knee joint model as very prospective.

Virtual knee model was built by using a PC-based system with the following configuration: 2 Intel Pentium Xenon 2.2 GHz processors, 1 GB RAM, and RAID 5 organisation of 120 GB hard discs. Processing accompanied by the reconstruction takes about 23 minutes on this PC system, modelling around 1 hour of manual work, while the simulation requires around 40 to 50 hours (300 simulation cycles). The later essentially depends upon specific patient anatomy, material properties, and force information used. The registration-reconstruction code is currently written just for single-processor computer systems; no speed up is thus expected if model construction is performed on multi-processor computer systems. Fortunately, there exist also multi-processor and cluster versions of the PAM Safe simulation tool. If simulation is run on 8-node cluster system, where each node has 2 processors, the calculated speed-up factor is then around 3 [15]. The most consumable construction part is thus reduced to 13 to 17 hours. The 8-node cluster system is optimal for our knee model consisting of a small number of FE elements. If a bigger cluster would be used, then execution times will be dominated by communication and no extra speed-up will be gained.

5 Discussion

Results of virtual human knee joint model were presented in the previous section. In the sequel, we will discuss the results, outline some problems and potential solutions for virtual model construction. Although discussion is bounded to human knee joint example, there are many suggestions and directives applicable to all similar applications.

Assessment of efficiency and accuracy of the constructed virtual medical model requires not only visual inspection, which provides just initial quality impression, but also thorough validation and verification. Figure 1 depicts that the construction of such models is a multi-step procedure. Thus, the final model depends upon all previous phases which must be evaluated as well. The error introduced in a particular processing phase is reflected also in the final model. It is very important to isolate potential sources of errors and to understand how this error is transferred through the processing chain. To achieve this, it is necessary to know the actual behaviour of the structure that is being modelled and the forces that it undergoes before it can be determined whether the behaviour of the model is valid.

The construction process begins with the patient-specific data. These data are usually considered completely valid. However, it is very common that some discrepancies occur during imaging. Errors introduced in this pre-phase are mainly neglected by the researchers, but such errors are extremely important because they can not be removed in subsequent phases. It is also very difficult to discover and correct these errors once imaging material is acquired and stored. A good idea is thus to record an entire process of patient material acquisition by a CCD camera, for example and, if in some later phase an error occurs in the imaging material, the entire acquisition process can be reviewed.

Construction of patient-specific knee joint model is not a completely automated procedure. Actually, it consists of two major building blocks (if we neglect imaging phase): registration-reconstruction part and modelling-simulation part. Image processing part is automated, while modelling phase requires user interaction. Modelling usually requires one hour of trained technician time. User must manually add some bars to the patient FE knee mesh and make some other corrections of the model. Fastening of elements (e.g. bars) to the mesh presents a potential source of errors, because the elements can be attached to wrong places. On the other hand, manual modelling is very flexible, as nearly any knee clinical case can be modelled (e.g. meniscus tear). However, from the verification point of view it is better that the construction tool is not so universal, but it supports a few checked construction scenarios. For a completely automated construction procedure, fastening points for ligaments and muscles should be detected in the image processing phase for each patient.

The registration routine used in the image processing phase (see Subsection 3.2.1) depends considerably upon MR scanner used in the imaging phase. It is known, that the variability inherent in MR imaging could cause the images of the same subject collected with the same MR protocol but with two different scanners may not be identical. Currently, this registration routine is fine tuned for the Toshiba Visart and Phillips Eclipse MR scanners. If knee joint images of other MR scanners are used, then an initialisation phase is required. This phase compensates variability found in the new type of images with regard to template image. This phase should theoretically be done just once per new type of MR scanner.

Modelling is the least deterministic phase in the entire process, because only a small portion of this phase is automated (e.g. assigning the material properties to elements), while the majority requires manual interaction. Modelling is to some extent intuitive (especially ligament and muscle fastening) and highly dependent upon the experts' knowledge and experience. This phase can not be verified directly. The only feedback is verification of simulation results. However, the verification just points out that there are some problems in the model, but it does not isolate sources of errors. In the current model, the verification is based just upon Euler rotation angles for bone tibia with respect to bone femur. It is thus suggested to expand verification also on the behaviour of other knee structures.

Stability of the patient FE knee mesh used in the modelling process is also very dependent upon the template mesh morphing and, indirectly, on the quality of the en-

tire image registration. For example, if the medial meniscus has been deformed considerably for particular patient, possibly due to actual pathology within the meniscus, the morphing algorithm will have to reduce the element sizes markedly. This by all means will not aid simulation stability. Therefore, it is possible that another manual intervention into modelling process may be necessary for gross knee pathologies.

In the sequel, the virtual human knee joint model is discussed from a medical point of view. Verification of the image processing part pointed out adequate accuracy of detected anatomical knee structures, especially in the orthopaedic surgeons target regions where the most pathologies occur (i.e. the condylar or articular and intercondylar region). The first benefit of knee model is thus an easy visualisation of detected knee structures in a particular cross section, even in anatomically problematic regions. In some cases, this "second opinion" could be of great help for clinicians in a preoperative planning and decision.

The simulated knee joint kinematics is almost realistic. In general, articular proportions in the simulated knee joint are very clear and no physiological structure deformations were detected. There are only some slight disturbances of the patella gliding at the extreme knee flexion, which might cause some disturbances in the patella kinematics. The shape and position of menisci are also very clear and no meniscus surface deformations are seen. The clinical benefit of the virtual knee joint model is also a better visualisation of the patient knee kinematics. For example, the knee could seem from MR images at first sight clinically stable, while the simulation points out enough functional instability. This was the case for a patient with partial anterior crucial ligament rupture, where suspicion on the ligament rupture was indicated only by the virtual knee model and confirmed by an arthroscopy examination. The knee instability was so big that the operative treatment was necessary.

Virtual knee joint model could have a big significance for planning operative interventions. It could be especially advantageous in the situations where postoperative knee joint stability and functionality is not obvious. When replacing a meniscus, for instance, a size of meniscus implant is selected by rule of thumb. Appropriateness of choice is usually confirmed about one year after operation. Thus, it is much better to play through different scenarios by using virtual model when taking such decisions.

The described virtual knee joint model has not been used in daily clinical practice yet. For such usage, this virtual model must be accompanied by several auxiliary tools. Visualisation tools and tools for correcting intermediate results are indispensable. Such tools should, for instance, visualize image registration results (i.e. 3D patient-specific knee mesh) and enable manual correction of particular segmentation results and, consequently, 3D knee mesh. Simulation results are currently visualized in the PAM View tool. The trained personnel only can interpret these results. More sophisticated model should also be accompanied by a tool for interpreting results from the medical point of view.

6 Conclusion

The framework for construction of patient-specific virtual medical models was presented in this paper. All construction blocks from imaging, image processing, modelling, and simulation were described and applicable directives issued. This framework was successfully applied by construction of virtual model of the human knee joint. Statistical assessment of the developed knee model pointed out sufficient accuracy of intermediate results and the final knee kinematics as well. This model was assessed also by the clinicians as very prospective.

Acknowledgement

This work was supported by the European funding in the 5th Framework project entitled SimBio (Contract No. IST-1999-10378).

References

[1] Ansys Inc., http://www.ansys.com/

[2] I.N. Bankman (2000), *Handbook of medical imaging: Processing and analysis*, Academic Press.

[3] C. Basdogan, C.-H. Ho, M.A. Srinivasan (2001), Virtual environments for medical training: graphical and haptic simulation of laparoscopic common bile duct exploration, *IEEE transactions on mechatronics*, vol. 6, no. 3, pp. 269–285.

[4] ESI group, PAM Suite, http://www.esi-group.com/

[5] E.M. Haacke, R.W. Brown, M.R. Thompson, R. Venkatesan (1999), *Magnetic resonance imaging: Physical principles and sequence design*, Wiley-Liss.

[6] J.V. Hajnal, D.L.G. Hill, D.J. Hawkes (2001), *Medical image registration*, CRC Press.

[7] T. He, L. Hong, D. Chen, Z. Liang (2001), Reliable path for virtual endoscopy: ensuring complete examination of human organs, *IEEE transactions on visualization and computer graphics*, vol. 7, no. 4, pp. 333–342.

[8] D. Korošec, A. Holobar, M. Divjak, D. Zazula (2003), Multilevel implementation of the dynamic virtual environment, *Proceedings of Fifth International Conference on Simulations in Biomedicine*, WIT Press, Southampton, pp. 477–486.

[9] J.-D. Lee, C.-H. Huang, S.-T. Lee (2002), Improving stereotactic surgery using 3-D reconstruction, *IEEE engineering in medicine and biology*, vol. 21, no. 6, pp. 109–116.

[10] A.D. McCarthy, D.R. Hose, D.C. Barber, S. Wood, G. Darwent, D. Chan, D.R. Bickerstaff, I.D. Wilkinson (2003), A registration-based MR method for calculating in-vivo 3-D knee joint motion: Validating finite element simulations, *Proceedings of the International society for magnetic resonance in medicine*, ISMRM, Toronto.

[11] H. Park, P. H. Bland, C.R. Meyer (2003), Construction of an abdominal atlas and its application in segmentation, *IEEE transaction on medical imaging*, vol. 22, no. 4, pp. 483–492

[12] B. Potočnik, D. Zazula (2001), Assessing the efficiency of the image segmentation algorithms, Electrotechnical review, vol. 68, no. 2/3, pp. 97-104.

[13] B. Potočnik, D. Zazula (2002), Automated analysis of a sequence of ovarian ultrasound images, Part I: Segmentation of single 2D images, *Image vision and computing* vol. 20, no. 3, pp. 217–225.

[14] B. Potočnik, D. Zazula (2002), Automated analysis of a sequence of ovarian ultrasound images, Part II: Prediction-based object recognition from a sequence of images, *Image vision and computing*, vol. 20, no. 3, pp. 227–235.

[15] SimBio project, http://www.simbio.de

[16] M. Sonka, V. Hlavac, R. Boyle (1994), *Image processing, analysis and machine vision*, Chapman and Hall.

[17] W. Sun, P. Lal (2002), Recent development on computer aided tissue engineeringŰŰa review, *Computer methods and programs in biomedicine*, vol. 67, no. 2, pp. 85–103.

[18] Surfdriver software, http://www.surfdriver.com/

[19] S. Wood, D.C. Barber, A.D. McCarthy, D. Chan, I.D. Wilkinson, G. Darwent, D.R. Hose (2002), A novel image registration application for the in vivo quantification of joint kinematics, *Proceedings of medical image understanding and analysis*, University of Portsmouth, Portsmouth.

[20] J. Xia, H.H.S. Ip, N. Samman, H.T.F. Wong, J. Gateno, W. Dongfeng, R.W.K. Yeung, C.S.B. Kot, H. Tideman (2001), Three-dimensional virtual-reality surgical planning and soft-tissue prediction for orthognathic surgery, *IEEE transactions on information technology in biomedicine*, vol. 5, no. 2, pp. 97–107.